Pharm Res (2013) 30:2036–2049
DOI 10.1007/s11095-013-1052-1

RESEARCH PAPER

Characterization of Damaged Skin by Impedance Spectroscopy: Mechanical Damage

Erick A. White • Mark E. Orazem • Annette L. Bunge

Received: 14 January 2013 / Accepted: 2 April 2013 / Published online: 25 May 2013

ABSTRACT

Purpose Electrochemical impedance spectroscopy is a convenient method that has been used to characterize skin barrier function, which affects drug delivery into and through the skin. The objective of this study was to relate changes in skin barrier function arising from mechanical damage to changes in the impedance spectra. These observations are compared in a companion paper to changes in chemically damaged skin.

Methods Electrical impedance and the permeation of a non-polar compound were measured before and after human cadaver skin was damaged by needle puncture.

Results The impedance responses of all skin samples were consistent with an equivalent circuit model with a resistor and constant phase element (CPE) in parallel. Pinhole-damaged skin exhibited a lower resistance pathway acting in parallel with the skin resistance without changing the CPE behavior. The characteristic frequency of the impedance scans determined after needle puncture increased by an amount that could be predicted. The flux of 4-cyanophenol increased by a small but significant amount that did not correlate with the hole resistance calculated under the assumption that the resistance of the surrounding skin did not change.

Conclusions Skin impedance measurements are sensitive to irreversible damage caused by exposure to puncture with a needle.

KEY WORDS constant phase element · impedance spectroscopy · pinhole · skin permeability · stratum corneum

ABBREVIATIONS

A	exposed skin area
CP	4-cyanophenol
CPE	constant phase element
C_s	capacitance of a capacitor in the R-C equivalent model circuit or an effective capacitance that is proportional to the effective dielectric constant
$C_{s,HM}$	effective capacitance for an R-CPE equivalent model circuit with the same characteristic frequency as the R-C circuit; described by Hsu and Manfeld (21)
$C_{s,OG}$	effective capacitance calculated by Oh and Guy (43, 44)
$C_{s,Oh}$	effective capacitance calculated by Oh *et al.*(10) and Kim and Oh (9)
$C_{s,PL}$	effective capacitance for an R-CPE equivalent model circuit with power-law decay of skin resistivity as proposed by Hirschorn *et al*. (38)
d_{hole}	diameter of pinhole
exp	experimental value
f	frequency of the potential (voltage) perturbation in the measurement of impedance
$f_{c,s}$	characteristic frequency observed for undamaged skin
$f_{c,t}$	characteristic frequency observed for pinhole damaged skin
f_k	k_{th} value of frequency measured
g	parameter in the definition for $C_{s,PL}$
Hz	Hertz, unit of frequency (cycles per sec)
j	$\sqrt{-1}$, unity in the complex plane
k	index of measurement frequency
L	thickness of the stratum corneum
L_{hole}	length of the pinhole in the skin
M	Cumulative mass of chemical delivered into the receptor solution at sample time t

Electronic supplementary material The online version of this article (doi:10.1007/s11095-013-1052-1) contains supplementary material, which is available to authorized users.

E. A. White · A. L. Bunge (✉)
Department of Chemical and Biological Engineering
Colorado School of Mines, 1500 Illinois Street
Golden, Colorado 80401, USA
e-mail: abunge@mines.edu

M. E. Orazem
Department of Chemical Engineering, University of Florida
Gainesville, Florida 32611, USA

Present Address:
E. A. White
ITN Energy Systems
Littleton, Colorado 80127, USA

N_{dat}	total number of measurement frequencies in the spectrum
nF	nanofarad, units of capacitance
N_{holes}	number of pinholes
N_{scans}	number of impedance scans included in the analysis of the stochastic error
P	parameter vector that includes all of the model parameter being optimized in the regression analysis
PBS	phosphate buffered saline
pK_a	negative of the base-10 logarithm of the acid dissociation constant, K_a
Q_s	parameter characterizing the constant phase element (CPE) in the equivalent circuit model of the stratum corneum
R-C	model circuit consisting of a resistor (R) and capacitor (C) in parallel
R-CPE	model circuit consisting of a resistor (R) and CPE in parallel
R_e	frequency-independent (Ohmic) resistance in series with the skin sample; consists of resistance of the electrolyte solution surrounding the skin sample, wires and possibly the dermis
R_{hole}	resistance of one hole
R_{holes}	resistance of N_{holes}
R_s	resistance of a resistor in the equivalent circuit model representing the stratum corneum
R_t	total resistance of the skin and hole operating in parallel
t	time
$\mathcal{Z}$	measured impedance; for an Ohmic material, the ratio of the current and potential by Ohms law; Z is a complex number
$\lvert\mathcal{Z}\rvert$	modulus of the impedance
$\mathcal{Z}_{exp}$	experimental value of the impedance, a complex number
$\mathcal{Z}_{MM}$	measurement model value of the impedance, a complex number
$\mathcal{Z}_j$	imaginary component of the impedance
$\mathcal{Z}_{j,exp}$	imaginary component of the experimental impedance
$\mathcal{Z}_r$	real component of the impedance
$\mathcal{Z}_{r,exp}$	real component of the experimental impedance
α_s	parameter characterizing the constant phase element (CPE) in the equivalent circuit model of the stratum corneum
δ	Distance from the outer surface to the innermost surface of the dominant resistive layer
ε	dielectric constant of the stratum corneum (unitless)
ε_0	permittivity of a vacuum, 8.8542×10^{-5} nF/cm
$\varepsilon_{res,m}$	frequency-dependent residual error of scan m defined as the difference between the measured and modeled impedance
$\overline{\varepsilon}_{res}(f_k)$	mean of the residual errors measured at frequency f_k for a number of scans (N_{scans})
Ω	ohms, units or resistance
$\theta_{c,s}$	phase angle at the characteristic frequency ($f_{c,s}$)
ρ	resistivity of solution surrounding the skin sample
ρ_δ	resistivity of the innermost surface of the dominant resistive layer
$\overline{\sigma}(f_k)$	average of the stochastic error at frequency f_k
σ	standard deviation of the stochastic error at frequency f_k
χ^2	objective function that is minimized in the data regression to the equivalent circuit model

INTRODUCTION

The outer most layer of the skin, the stratum corneum, is a matrix of dead keratinized cells suspended in lipid bilayers. The stratum corneum is the primary barrier to chemical penetration and electric current through the skin. Therefore, unless stated otherwise, in this paper the word skin refers to the stratum corneum. Impedance spectroscopy, which is the measurement of the impedance for a range of frequencies, provides information about the electrical properties of skin. Impedance measurements involve measuring the current or potential response to small-amplitude modulation of an input current or potential at a given frequency. The impedance is the ratio of the change in potential to the change in current, which for skin is a function of the modulation frequency. Dielectric material in skin causes the resulting signal to shift in phase relative to the applied signal, which can be expressed as a complex number for impedance. Changes in the impedance spectra of skin subsequent to chemical exposure or mechanical damage indicate changes in the structure or composition of skin.

The electrical response of the skin is related to two intrinsic properties: the resistivity and the dielectric constant. The skin resistivity is proportional to the area-normalized skin resistance measured using a direct current method; *i.e.*, $R_s A$ where A is the skin area normal to current flow and R_s is the skin resistance with units of Ohms. The dielectric constant of skin is proportional to the capacitance normalized by the inverse area (C_s/A). Because the stratum corneum is heterogeneous, macroscopic electrical measurements of the skin produce effective values for the skin resistance and capacitance that combine effects from the various structures within the stratum corneum. Hydrophilic and lipophilic molecules diffuse through skin *via* polar or nonpolar pathways depending upon the octanol-water partition coefficient (1). For skin submerged in electrolyte solution, dissolved ions transport through the skin in response to an electric field. Thus, skin resistivity quantitatively characterizes the pathway for transport of ions through skin. Consistent with this, the skin permeability of hydrophilic and ionic chemicals, including water, has been shown to be inversely proportional to $R_s A$; *e.g.* (2–6).

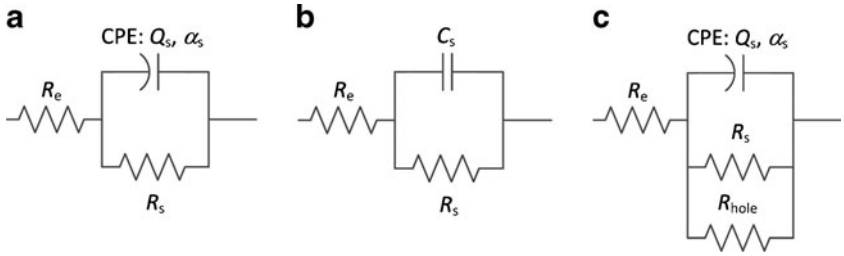

Fig. 1 Diagrams of equivalent circuit models: (**a**) R-CPE model, (**b**) R-C model, and (**c**) R-CPE pinhole model.

Though the source of skin capacitance is not well understood, investigators have speculated that the skin capacitance arises from reorientation of polar lipids and proteins in the electric field (7) and the lipid matrix-keratin cell complex elements (8–11) that might act as insulating layers of highly ordered stratum corneum lipids separated by conducting corneocytes. Since the stratum corneum lipids are thought to be the major component of the lipophilic pathway, the effective capacitance of skin may in some ways characterize the lipophilic pathway.

The present work was one of two studies that had the overall goal of using impedance spectroscopy to characterize and understand changes in skin barrier function following irreversible damage. The objective of the present study was to examine changes in the impedance response and the permeation of a non-polar model compound, 4-cyanophenol (CP), to a well-defined mechanical insult, specifically needle puncture. Electrical impedance is one of the recommended methods for insuring that skin samples have sufficient integrity for meaningful *in vitro* measurements of chemical permeability, including non-polar compounds (12–14). Therefore, a secondary objective was to compare the effects of pinhole damage on electrical impedance and CP permeation. This understanding of mechanical damage informed the second study, described in a companion paper, in which impedance spectroscopy was determined before and after skin was damaged chemically using dimethyl sulfoxide (15). The strategy in both investigations was to derive insights into the intrinsic electrical properties of skin before and after damage by regressing circuit models that are consistent with the nature of the skin damage to the measured impedance.

THEORY

Skin impedance is related to the structure and composition of the stratum corneum. In the present study the skin barrier was damaged mechanically by needle puncture. Circuit models are proposed to describe the resulting skin impedance.

Skin Impedance Models

A common circuit model of *in-vitro* skin impedance is a resistor that represents the frequency-independent (Ohmic) resistance containing contributions from the electrolyte, the wires, and possibly the dermis (R_e) in series with a parallel resistor (R_s) and a constant-phase element (CPE) (16, 17). This R-CPE circuit model is depicted in Fig. 1a. The CPE is often thought of as being a non-ideal capacitor, with a complex impedance given by

$$\mathcal{Z} = \frac{1}{Q_s (j2\pi f)^{\alpha_s}} \tag{1}$$

where Q_s and α_s are the CPE parameters, j is the complex number $\sqrt{-1}$, and f is the frequency with units of inverse seconds (Hz). Jorcin *et al.* (18) demonstrated that, in general, CPE behavior can be the result of surface and normal (or axial) distributions of resistance and capacitance in the material. In skin, the CPE behavior has been attributed to the stratum corneum heterogeneity normal to the skin surface, particularly an exponential decrease in the resistivity (19, 20).

The impedance of the R-CPE model is represented by the expression

$$\mathcal{Z} = R_e + \frac{R_s}{1 + R_s Q_s (j2\pi f)^{\alpha_s}} \tag{2}$$

which exhibits a single characteristic frequency, $f_{c,s}$, defined as

$$f_{c,s} = \frac{1}{2\pi (R_s Q_s)^{1/\alpha_s}} \tag{3}$$

corresponding to the frequency at which the absolute value of the imaginary part of the impedance is a maximum. Since the dielectric constant for a material is linked to the capacitance, it is useful to relate the parameters in the R-CPE model to an effective capacitance. In one approach, the R-CPE model is related to the R-C circuit model, shown in Fig. 1b. In this circuit, a resistor is in series with a parallel resistor (R_s) and capacitor (C_s), which is represented exactly by Eq. (2) for $Q_s = C_s$ and $\alpha_s = 1$. The effective capacitance is determined by requiring that the characteristic frequency for the R-C circuit model

$$f_{c,s} = \frac{1}{2\pi R_s C_s} \tag{4}$$

is the same as the characteristic frequency for the R-CPE model; *i.e.*, Eq. (3). The resulting expression,

$$C_{s,HM} = Q_s^{1/\alpha_s} R_s^{(1-\alpha_s)/\alpha_s} \tag{5}$$

is derived by equating Eqs. (3) and (4) and solving for C_s in terms of R_s, Q_s and α_s. All effective capacitance values derived from CPE parameters are model dependent and as Eq. (5) has been described by Hsu and Mansfeld (21), the effective capacitance calculated using Eq. (5) is designated as $C_{s,HM}$ to distinguish it from values calculated by other approaches.

The impedance of punctured skin, shown schematically in Fig. 2, is hypothesized to vary with frequency as described by the pinhole equivalent circuit depicted in Fig. 1c and represented by

$$\mathcal{Z} = R_e + \frac{R_t}{1 + R_t Q_s (j2\pi f)^{\alpha_s}} \tag{6}$$

where Q_s and α_s are the CPE parameters of the skin after the hole was punctured, and R_t is the total resistance of the skin and hole operating in parallel, *i.e.*

$$R_t = \left[\frac{1}{R_s} + \frac{1}{R_{hole}}\right]^{-1} \tag{7}$$

Like undamaged stratum corneum, the pinhole equivalent circuit model is characterized by a single characteristic frequency, $f_{c,t}$, given by

$$f_{c,t} = \frac{1}{2\pi (R_t Q_s)^{1/\alpha_s}} \tag{8}$$

From the characteristic frequency of the corresponding R-C circuit,

$$f_{c,t} = \frac{1}{2\pi R_t C_s} \tag{9}$$

the effective capacitance of the punctured skin, $C_{s,HM}$, is derived to be:

$$C_{s,HM} = Q_s^{1/\alpha_s} R_t^{(1-\alpha_s)/\alpha_s} \tag{10}$$

using the procedure described above for R-CPE model. If the cross-sectional area of the hole is small compared to the skin area, then the skin resistance (R_s) and the dielectric constant of the skin before and after the pinhole are expected to be the same. If $C_{s,HM}$ represents the effective dielectric constant of the stratum corneum, it follows that $C_{s,HM}$, measured before and after the skin is punctured should also be the same.

Model Calculations

Log-log graphs of the real and imaginary components of the impedance (*i.e.*, $\mathcal{Z}_r A$ and $-\mathcal{Z}_j A$), plotted as a function of frequency, each reveal different features of the impedance response or circuit model. For all circuit models shown in Fig. 1, the real component of the impedance approaches the total resistance of the sample at low frequencies (*i.e.*, $(R_e + R_s) A$ and $(R_e + R_t) A$ for undamaged and damaged skin, respectively) and R_e at high frequencies. Also for these circuit models, the maximum value of $-\mathcal{Z}_j A$ occurs at the characteristic frequency. For the R-CPE and pinhole models, the slope of $-\mathcal{Z}_j A$ *versus* frequency approaches α_s and $-\alpha_s$, respectively at frequencies that are smaller and larger than the characteristic frequency (22). For the R-C model, the slope $-\mathcal{Z}_j A$ *versus* frequency approaches 1 and −1, respectively.

Occasionally, features that cannot be identified in the two plots described above are evident in a graph of the first derivative of $\log(-\mathcal{Z}_j A)$ with respect to $\log(f)$ plotted as a function of frequency (23). The derivative is estimated numerically by the following difference equation

$$\frac{d\log(-\mathcal{Z}_j A)}{d\log(f)} = \frac{\log(-\mathcal{Z}_j A)_k - \log(-\mathcal{Z}_j A)_{k-1}}{\log(f)_k - \log(f)_{k-1}} \tag{11}$$

where k and k-1 are the indices of measurements at adjacent frequencies. Equation (11) represents a central difference formula when $\log(f)$ is given by

$$\log(f) = \frac{\log(f_{k-1}) + \log(f_k)}{2} \tag{12}$$

For the R-CPE model given by Eq. (2), $d\log(-\mathcal{Z}_j A)/d\log(f)$ asymptotically approaches α_s at low frequencies and $-\alpha_s$ at high frequencies, and equals zero at the characteristic frequency. Perturbations to this behavior in the form of inflection points or local minimum and maximum occur if the spectrum is inconsistent with a circuit model described by a single characteristic frequency.

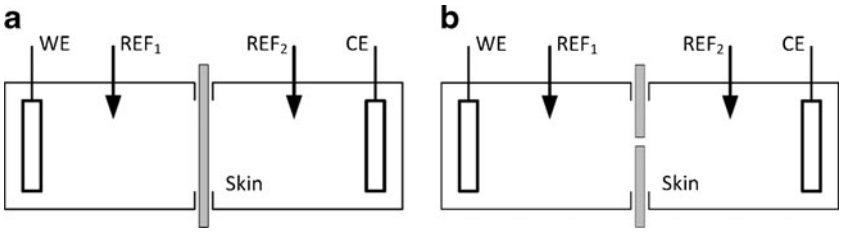

Fig. 2 Schematic representation of the measurement of skin impedance with four-electrode measurement of: (**a**) intact piece of skin; and (**b**) skin punctured by a needle.

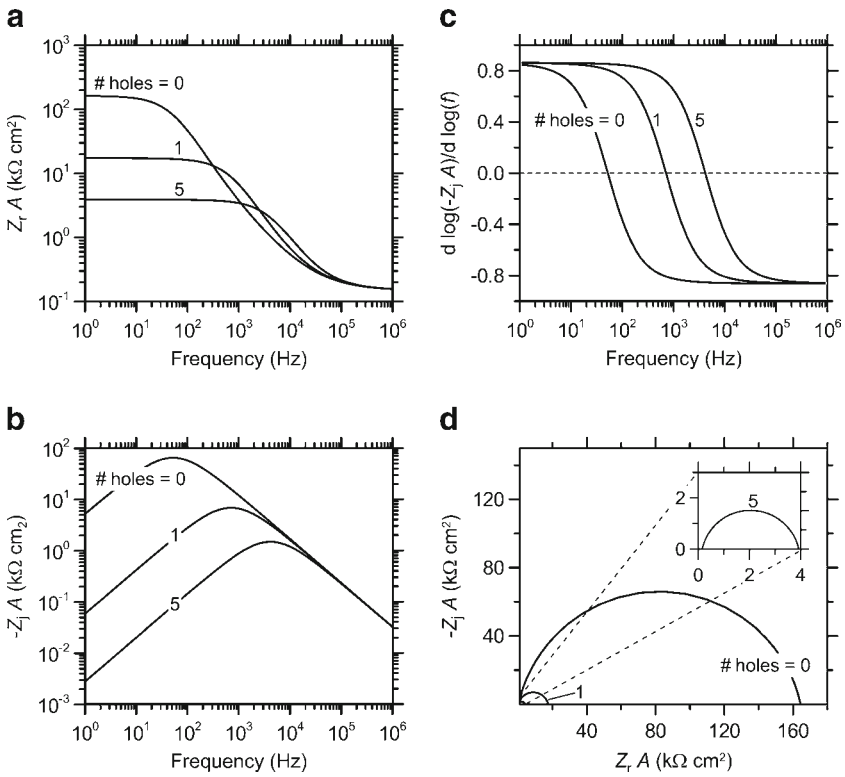

Fig. 3 Impedance spectra calculated using the pinhole model for varying numbers of holes and typical values of the model parameters in this study: $R_e A = 0.15\ \text{k}\Omega\ \text{cm}^2$, $R_s A = 167.0\ \text{k}\Omega\ \text{cm}^2$, $Q_s/A = 41.4\ \text{nF}\ \text{s}^{\alpha_s-1}/\text{cm}^2$, $\alpha_s = 0.862$, $f_{c,s} = 51$ Hz and $R_{hole} A = 19.3\ \text{k}\Omega\ \text{cm}^2$ in a diffusion cell with $A = 1.65\ \text{cm}^2$.

The graphical features of these plots are illustrated in Fig. 3 for the pinhole model. Using Eq. (6), $\mathcal{Z}_r A$ and $-\mathcal{Z}_j A$ were calculated as a function of frequency for input parameter values that are reasonable for undamaged skin ($R_s A = 167.0\ \text{k}\Omega\ \text{cm}^2$, $\alpha_s = 0.862$, $Q_s/A = 41.4\ \text{nF}\ \text{s}^{\alpha_s-1}/\text{cm}^2$, and $f_{c,s} = 51$ Hz). Calculated results are shown for the number of holes varying from 0 to 5 under the assumptions that each hole did not influence the impedance of the other holes, and that adding holes did not change the R-CPE parameters of the skin (*i.e.*, R_s, Q_s and α_s were assumed to be constant). Each hole acted in parallel to the skin resistance with an assumed resistance normalized by the exposed skin area ($R_{hole}\ A$) equal to 19.3 $\text{k}\Omega\ \text{cm}^2$ in a diffusion cell with $A = 1.65\ \text{cm}^2$, which is similar to what was seen in the experiments with one hole described below (*i.e.*, sample 3). Therefore, the total resistance attributed to the holes (R_{holes}) is the resistance of one hole (R_{hole}) divided by the number of all holes ($\mathcal{N}_{holes}$) as follows:

$$R_{holes} = \frac{R_{hole}}{\mathcal{N}_{holes}} \tag{13}$$

The resistance for $\mathcal{N}_{holes}$ is equivalent to the resistance of one hole with a cross-sectional area that is larger by a factor of $\mathcal{N}_{holes}$ than the area of the hole with a resistance R_{hole}.

As shown in Fig. 3, the total resistance, indicated by $\mathcal{Z}_r A$ at low frequency, decreased with an increasing number of pinholes while the characteristic frequency, which is the frequency at which the $-\mathcal{Z}_j A$ curves are maximized or where $\text{d}\log(-\mathcal{Z}_j A)/\text{d}\log(f)$ equals zero, increased with the number of holes. Increasing the number of pinholes reduced the total resistance of the system causing the characteristic frequency to increase. Consistent with a circuit characterized by a single characteristic frequency, plots of $\text{d}\log(-\mathcal{Z}_j A)/\text{d}\log(f)$ decrease monotonically with frequency from α_s to $-\alpha_s$, crossing zero at $f = f_{c,t}$.

Impedance plane plots, sometimes called Nyquist plots, are also used to present impedance data. In this plot (Fig. 3d), $-\mathcal{Z}_j A$ is graphed as a function of $\mathcal{Z}_r A$ on linear axes. For the R-CPE and pinhole circuit models, the plot looks like a single depressed semi-circle in which the maximum value of $-\mathcal{Z}_j A$ is less than half the difference of the maximum and minimum values of $\mathcal{Z}_r A$. The degree to which the plot deviates from a perfect semi-circle, which occurs when α_s is exactly equal to one, depends on how much α_s deviates from unity. The low-frequency data appear on the right side of the $\mathcal{Z}_r A$ axis and the frequency increases towards the left. Thus, the low and high-impedance intercepts of the $\mathcal{Z}_r A$ axis, which correspond to high and low frequency, are equal to $R_e A$ and the total resistance of the system (*i.e.*, $(R_e + R_s) A$ for undamaged skin and $(R_t + R_s) A$ for damaged skin). The impedance values corresponding to the characteristic frequency appear at the top of the semi-circle (*i.e.* where $-\mathcal{Z}_j A$ is a maximum). Deviations from the semi-circular behavior illustrated in Fig. 3d would indicate a spectrum that is inconsistent with a circuit model described by a single characteristic frequency.

MATERIALS AND METHODS

Chemical flux and impedance spectra were measured before and after skin was damaged by needle puncture. The experimental procedures for these studies and the related determination of solution resistivity are described below.

Chemicals and Materials

Phosphate buffered saline (0.01 M) with 0.138 M NaCl, 0.0027 M KCl (pH 7.4, Sigma P-3813) was prepared in deionized (DI) water (Millipore Corporation, Bedford, MA). The permeation of 4-cyanophenol (CAS 767-00-0, molecular weight = 119.1 Da, logarithm of the octanol-water partition coefficient = 1.6, and $pK_a = 7.97$) purchased from Sigma was measured before and after skin was punctured with a needle (26S gauge, Hamilton CO., Reno, NV). Split-thickness human cadaver skin (300–400 μm thick) identified as Q (from the back of a 77-year old Caucasian female) and AS (from either the back or abdomen of a 78-year old Caucasian male) was purchased from the National Disease Research Interchange (NDRI, Philadelphia, PA). The skin was collected within 24 h post mortem, frozen immediately and stored at temperatures lower than −60°C until used.

Diffusion Cell Apparatus

Skin impedance and chemical flux were both measured in horizontally oriented glass diffusion cells from PermeGear (13 mL, Side-Bi-Side™ diffusion cells, Hellertown, PA) adapted to allow 4-electrode impedance measurements and to support the skin sample during manipulations requiring it to be removed from the cell. Each skin sample was mounted into one of four custom-made frames (the diffusion area was 1.84 cm^2 for one 1.65 cm^2 for the other three) constructed PDM Services, Golden, CO. This frame fit between the two diffusion cell chambers that each held two Ag/AgCl electrodes (*In Vivo* Meteric, Healdsburg, CA): one working electrode (WE) and one reference electrode (REF) as shown in Fig. 2. The working electrodes were 12-mm diameter discs oriented with the face parallel to the skin surface. The cylindrical reference electrodes (1.5 mm diameter and 3 mm long) were oriented such that the long axis was parallel to the skin surface. Experiments were conducted in a temperature-controlled chamber (Electro-Tech Systems, Inc., PA) that was large enough to hold all four cells and maintained at 32°C.

Skin Impedance Measurements

Impedance was measured using a Gamry potentiostat (model PCI4/300, Warminster, PA). A 10 mV root-mean-squared, sinusoidal alternating current perturbation signal with a mean applied potential of zero (*i.e.*, no direct current bias) was applied at 10 frequencies per logarithmic decade over the frequency range of 0.1 Hz to 20 kHz.

Pinhole Experiments

After the frame holding the skin was clamped into a diffusion cell, both chambers were filled with PBS for an eight to twelve hour equilibration period. During the equilibration period, impedance spectra were measured hourly to establish a baseline for the electrical properties of the skin as well as to verify that the skin was at equilibrium as indicated by insignificant differences between subsequent spectra.

After equilibration, solutions from both chambers were drained and 13 mL of PBS and PBS saturated with 4-cyanophenol (CP) were placed into the receptor chamber and donor chambers, respectively. To ensure saturation of the donor solution throughout the experiment, excess crystals of CP were added to the donor chamber solution. Either 1 or 2-mL samples were collected hourly from the receptor solution with replacement starting 4 h after introducing the saturated donor solution and continuing for 3 h. After this, the frame holding the skin was removed from the diffusion cells, a hole was poked with the needle (464 μm outside diameter), the diffusion cell was reassembled, and the donor and receptor chambers refilled with fresh CP-saturated PBS and PBS, respectively. Seven 2-mL samples were collected from the receptor chamber with replacement every 0.75 h after introducing the CP donor solution. Impedance spectra were collected hourly during the flux measurements and results reported before and after needle puncture were derived from the last spectrum collected during the CP flux measurements. A control experiment was performed in which one skin sample from subject Q was treated in the same way as the other samples except that it was not punctured.

Concentrations of CP in the collected solutions were measured using a high-performance liquid chromatograph (HPLC, Hewlett Packard 1100, Palo Alto, CA) equipped with auto-sampling and a diode array detector set to 254 nm. The stationary phase was a Zorbax Extend-C18 (4.6 × 250 mm, Agilent Technologies, Santa Clara, CA) column. The mobile phase was acetonitrile and water (70:30 v:v) flowing at 1 mL/min, which gave a retention time of about 2.3 min. Calibration using 4 or 5 standards was conducted prior to chemical analysis, with concentrations that encompassed the range of sample concentrations. The limit of reliable quantification was approximately 0.1 μg/mL.

Steady-State Flux Determination

The cumulative mass of chemical delivered into the receptor solution (M) at a sample time (t) was calculated by summing

the mass of chemical in the receptor chamber and the total mass of chemical removed from the receptor solution in previous samples. The mass of chemical in the receptor chamber at t is the product of the receptor solution volume and the measured chemical concentration in the sample collected at time t. The mass removed from the receptor chamber by sampling is the product of the concentration and volume of the sample.

The steady-state flux which is the slope of the linear portion of the area normalized cumulative mass (M/A) *versus* t curve, was determined by linear regression. In determining CP flux before pinhole damage, the skin had not been exposed previously to CP and the intercept of the regressed line to the time axis is the lag time. Experimental estimates for steady-state flux that include M/A measurements at times less than about 2.4 times the lag time are systematically lower than the actual value (24); thus, data points collected before 2.4 times the lag time were removed and the regression was repeated. Typically, steady-state is reached within 2 to 4 h. Steady-state flux was established sooner than this in the pinhole damaged skin, which contained CP from the before damage measurement. In most cases, the steady-state flux was determined using at least four data points; in all cases, at least three data points were used.

Solution Resistivity Measurements

The resistivity of the PBS solution at 32°C was determined to be 54.855±0.003 Ω cm (mean ± one standard deviation, $n=6$) by measuring the resistance of the PBS solution in one of the diffusion cells containing no skin and filled with 26 mL of PBS. Six successive impedance spectra of frequencies between 1 Hz and 100 kHz were measured in the four electrode configuration. The resistance from each spectrum was the average value of Z_r measured at frequencies where only the resistance of the PBS solution contributed to the impedance response of the system as indicated by $-Z_j=0$ (typically between 10 and 300 Hz). The average resistance of the six scans across the cross-section area of the diffusion cell was 93.623±0.005 Ω cm^2 (mean ± one standard deviation). The resistivity was calculated from the product of this resistance and the electrode cell constant, which accounts for the effective area and length of the solution between the electrodes in the diffusion cell relative to the cross-sectional area of the diffusion cell. The cell constant was determined by measuring the resistance of standard solutions (0.01, 0.1 and 1 molal potassium chloride in DI water) with known resistivity at 32°C (8.19, 68.68 and 623.91 Ω cm, respectively from Pratt *et al.* (25)) in the same diffusion cell by the procedure described above. The cell constants for the three solutions, calculated from the ratio of the resistivity to the measured resistance, were independent of the potassium chloride concentration and equal to 0.586 ±0.005 cm (average ± standard deviation).

Regression Analysis

Equations representing the chosen equivalent circuit model were regressed to the complex impedance data by minimization of the objective function (χ^2) defined as:

$$\chi^2(\mathbf{P}) = \sum_{k=1}^{N_{dat}} \left[\frac{\left(Z_{r,exp}(f_k) - Z_r(f_k|\mathbf{P})\right)^2 + \left(Z_{j,exp}(f_k) - Z_j(f_k|\mathbf{P})\right)^2}{\overline{\sigma}(f_k)^2} \right] \tag{14}$$

In this expression k is an index for the observation at each measurement frequency f_k, N_{dat} is the total number of measurement frequencies in the spectrum, $Z_{r,exp}(f_k)$ and $Z_{j,exp}(f_k)$ are the real and imaginary experimental impedance data measured at frequencies f_k, $Z_r(f_k|\mathbf{P})$ and $Z_j(f_k|\mathbf{P})$ are the real and imaginary parts of the equivalent circuit model equation evaluated at frequency f_k for the parameter vector $\mathbf{P}$ (which includes all of the model parameters being optimized), and $\overline{\sigma}(f_k)$ is the average of the stochastic error at frequency f_k determined as described below. The errors reported for tabulated values of the regressed parameters are the asymptotic standard parameter errors, which is the square root of the covariance matrix (26). The objective function was minimized using a Levenberg-Marquardt algorithm developed and implemented in MatLab^{TM} by Gavin (26). Orazem and Tribollet (27) provide a description of the Levenberg-Marquardt method for regression to complex numbers.

The stochastic error in the measurements at each frequency $\overline{\sigma}(f_k)^2$ was estimated from the average of the stochastic error of the real (σ_r) and imaginary (σ_j) parts of the measured impedance at frequency f_k. The σ_r and σ_j were estimated following the measurement model approach described in the papers by Agarwal *et al.* (28–31) and Orazem *et al.* (32). This involves fitting the impedance data to a simple equivalent circuit model (also known as the measurement model) consisting of an optimal number of R-C circuits in series to five successive impedance spectra by modulus-weighted, complex non-linear least squares regression using the Measurement Model Toolbox developed by Orazem (33). The residual error between the data and the measurement model cannot be taken as the stochastic error because the error due to lack of fit could be significant. However, the standard deviation of the residuals, expressed in terms of the mean of the residual errors at frequency f_k ($\overline{\varepsilon}_{res}(f_k)$) for all scans ($N_{scans}$) included in the analysis (*i.e.*, $N_{scans}=5$ in this study) as

$$\sigma^2(f_k) = \frac{1}{N_{scans}-1} \sum_{m=1}^{N_{scans}} \left(\varepsilon_{res,m}(f_k) - \overline{\varepsilon}_{res}(f_k)\right)^2 \tag{15}$$

is an estimate of the standard deviation of the stochastic error as a function of frequency where $\varepsilon_{\mathrm{res,m}}(f_k)$ is the residual error of either the real or imaginary part of the impedance at frequency f_k of scan m, defined as

$$\varepsilon_{\mathrm{res,m}}(f_k) = \mathcal{Z}_{\exp}(f_k) - \mathcal{Z}_{\mathrm{MM}}(f_k) \tag{16}$$

In Eq. (16), $\mathcal{Z}_{\exp}(f_k)$ is the experimentally measured value of the impedance and $\mathcal{Z}_{\mathrm{MM}}(f_k)$ is the impedance calculated from the measurement model at frequency f_k for the optimal number of R-C circuits in series.

RESULTS AND DISCUSSION

The low-frequency impedance response is analyzed in this section in terms of an effective pinhole diameter. Analysis of different estimations of effective capacitance reveals that a formula based on the high-frequency impedance response yields more reliable values of dielectric constant than do formulas derived from the characteristic frequency. The steady-state flux of CP is seen to be relatively insensitive to needle puncture; whereas, the impedance response shows substantial sensitivity.

Skin Impedance

Typical impedance spectra measured before and after needle puncture are shown in Fig. 4 for sample 4 along with theoretical curves derived by regression to the R-CPE and pinhole models. Values of the model parameters determined by regression of impedance measurements before and after pinhole damage for sample 4 and six others are listed in Table I. In Table II regression parameters are reported for the control experiment, in which a skin sample was treated in the same way as the other samples except that it was not punctured. The impedance responses of all skin samples, both before and after pinhole damage, were adequately represented by the R-CPE and pinhole models as illustrated by the good agreement between the impedance models and data in Fig. 4 except at the lowest frequency values for $-\mathcal{Z}_j A$. This deviation, which has no effect on the regressed parameter values, arises because the magnitude of $-\mathcal{Z}_j A$ at low frequencies is small enough to be affected by instrument noise. Values for R_e have not been reported because impedance was not measured at high enough frequencies to obtain a reliable estimate for its value by fitting the R-CPE model.

Because the needle used to puncture the skin was small compared to the total skin area, the pinhole was expected to have little effect on the impedance properties of the remaining skin. From the control experimental results (Table II), it was confirmed that the electrical properties of skin did not change during the other skin handling steps. Therefore, the resistance and the dielectric constant for the skin were assumed to be the same before and after pinhole. Consistent with the hypothesis that pinhole damage only adds a low frequency shunt resistance (*i.e.*, R_{hole}) in parallel with the skin resistance, after pinhole damage the resistance changed while the CPE parameters, α_s and Q_s, did not. The average resistance before pinhole damage was almost 10 times larger and more variable

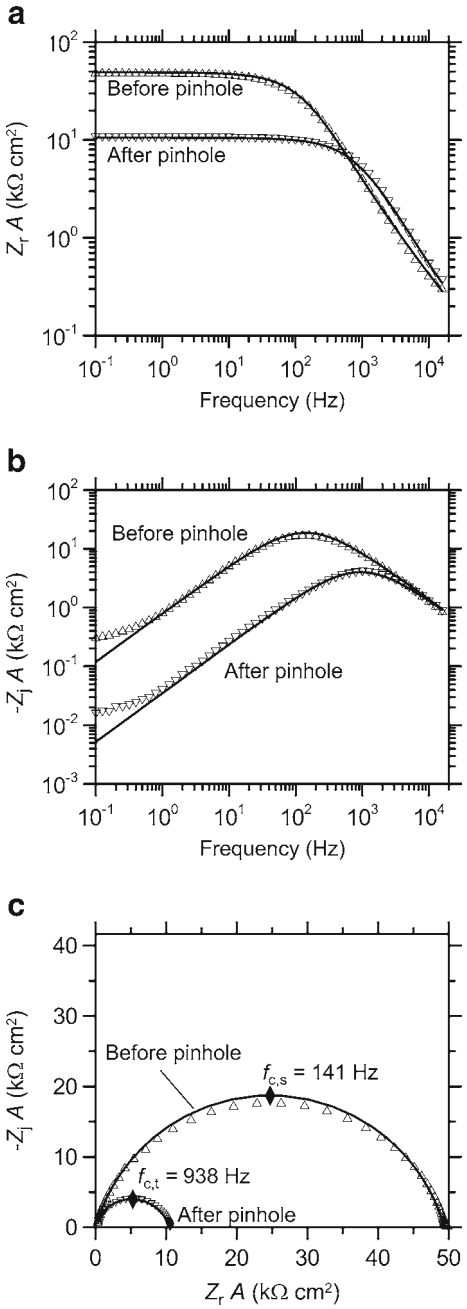

Fig. 4 Typical impedance spectra measured before and after addition of a pinhole for sample 4 compared with R-CPE models (*solid lines*) for skin with and without a pinhole: (**a**) area normalized real part of the impedance, (**b**) area normalized imaginary part of the impedance, and (**c**) impedance plane (Nyquist) plot with the impedance values at the characteristic frequencies denoted with diamonds.

Table I Parameter Values for the R-CPE and Pinhole Models Regressed Respectively to Skin Data Before and After Damage with One Pinhole, and Estimates of the Pinhole Resistance and Diameter

Parameter	Units	Sample ID[a] 1		2		3		4	
		Before	After	Before	After	Before	After	Before	After
Regressed parameters[b]									
$R_s A$[c]	kΩ cm^2	141.8 ± 0.2		93.6 ± 0.1		93.4 ± 0.1		55.2 ± 0.1	
$R_t A$	kΩ cm^2		9.94 ± 0.01		24.07 ± 0.03		15.96 ± 0.02		11.78 ± 0.01
α_s	unitless	0.81 ± 0.002	0.82 ± 0.002	0.82 ± 0.01	0.82 ± 0.003	0.79 ± 0.01	0.82 ± 0.003	0.83 ± 0.01	0.83 ± 0.002
Q_s/A	nF s$^{\alpha_s-1}$/cm^2	79.8 ± 1.0	67.7 ± 1.5	68.5 ± 1.3	73.5 ± 1.4	99.7 ± 1.1	83.0 ± 1.4	66.5 ± 1.4	63.7 ± 1.1
Calculated parameters[d]									
$R_{hole} A$[e]	kΩ cm^2		10.7 ± 0.01		32.4 ± 0.07		19.3 ± 0.03		15.0 ± 0.02
R_{hole}	kΩ		6.48 ± 0.01		19.76 ± 0.04		11.67 ± 0.02		8.14 ± 0.01
$f_{c,s}$ or $f_{c,t}$[f]	Hz	41 ± 0.2	1117 ± 1.1	74 ± 1	364 ± 0.5	59 ± 1	528 ± 0.6	141 ± 1	938 ± 1.0
d_{hole}[g]	μm		241		126		170		210

Parameter	Units	Sample ID[a] 5		6		7		All samples[h]	
		Before	After	Before	After	Before	After	Before	After
Regressed parameters[b]									
$R_s A$[c]	kΩ cm^2	179 ± 0.3		192 ± 0.3		69.2 ± 0.1		118 ± 54	
$R_t A$	kΩ cm^2		15.63 ± 0.02		21.20 ± 0.04		14.88 ± 0.02		16.21 ± 4.96
α_s	unitless	0.83 ± 0.01	0.85 ± 0.003	0.81 ± 0.01	0.84 ± 0.004	0.82 ± 0.01	0.83 ± 0.003	0.80 ± 0.01	0.83 ± 0.01
Q_s/A	nF s$^{\alpha_s-1}$/cm^2	61.8 ± 1.2	51.3 ± 0.9	70.5 ± 1.2	57.3 ± 1.3	74.3 ± 1.7	69.5 ± 1.3	74.4 ± 12.5	66.6 ± 10.5
Calculated parameters[d]									
$R_{hole} A$[e]	kΩ cm^2		17.1 ± 0.02		23.8 ± 0.05		19.0 ± 0.03		19.6 ± 6.9
R_{hole}	kΩ		10.38 ± 0.01		14.54 ± 0.03		10.30 ± 0.02		11.6 ± 4.4
$f_{c,s}$ or $f_{c,t}$[f]	Hz	37 ± 1.0	721 ± 0.9	31 ± 0	477 ± 0.8	98 ± 1	648 ± 0.8	68.7 ± 39.4	685 ± 266
d_{hole}[g]	μm		182		150		183		180 ± 35

[a] Samples 1–4 are from subject Q; samples 5–7 are from subject AS

[b] Values are reported as the regressed parameters ± the standard parameter error

[c] $R_s A$ before and after pinhole damage is assumed to be unchanged for purposes of calculating R_{hole}

[d] Values are reported as the calculated parameter ± the error estimated by propagation of the standard parameter error on the regressed parameters contained in the calculated parameter (27)

[e] $R_{hole} A$ is calculated from $R_t A$ and $R_s A$ according to Eq. (7)

[f] $f_{c,s}$ and $f_{c,t}$ for skin before and after pinhole damage, respectively are calculated from Q_s and either R_s or R_t as specified in Eqs. (3) and (8)

[g] Hole diameter was estimated using Eq. (17)

[h] Values are the mean and one standard deviation of the parameter value for all seven skin samples

than after pinhole damage (*cf.* 118±54 kΩ cm^2 compared with 16.21±4.96 kΩ cm^2; mean ± standard deviation for n=7). In contrast, the variability in the CPE parameters for all 16 measurements listed in Tables I and II, including skin with and without pinholes, was relatively smaller: α_s=0.82±0.01 and Q_s/A=72±12 nF s$^{\alpha_s-1}$/cm^2 (mean ± standard deviation).

Values for the resistance of the pinhole, R_{hole}, listed in Table I were calculated by rearrangement of Eq. (7) under the assumption that $R_s A$ was equal to the before pinhole value. The resistance R_{hole} is related to the solution resistivity (ρ), the hole diameter (d_{hole}) and the length of the hole (L_{hole}) as

$$R_{hole} = \frac{\rho}{2d_{hole}} + \frac{4L_{hole}\rho}{\pi d_{hole}^2} \quad (17)$$

where the first term on the right hand side represents the constriction of the flux lines from a semi-infinite bulk electrolyte solution to the hole, and the second term represents the resistance of the electrolyte solution in the hole when the surrounding skin is impermeable to ions (34, 35). Under the

Table II Parameter Values of the R-CPE Model Regressed to Skin Data for the Control Sample Before and After Damage with One Pinhole[a]

Parameter[b]	Units	Before	After
$R_t A$	kΩ cm^2	103.2 ± 0.2	102.6 ± 0.16
α_s	Unitless	0.80 ± 0.002	0.81 ± 0.002
Q_s/A	nF s$^{\alpha_s-1}$/cm^2	85.6 ± 1	83 ± 1
$f_{c,s}$	Hz	58 ± 0.1	58 ± 0.1

[a] One skin sample from subject Q was treated the same as all other skin samples in the pinhole experiment but without puncturing a hole

[b] Values of all parameters except the characteristic frequency ($f_{c,s}$) are reported as the regressed parameter ± the standard parameter error. Values of $f_{c,s}$ are reported as the calculated parameter ± the error estimated by propagation of the standard parameter error on the regressed parameters contained in the calculated parameter (27)

assumption that the pinhole was completely filled with PBS solution, the effective diameter of the pinhole, d_{hole}, for each sample was estimated from R_{hole} using the measured resistivity of PBS solution (ρ=54.9 Ω cm) and the total thickness of the skin sample (*i.e.*, approximately 350 μm for the split-thickness skin used in this study).

Calculated values for d_{hole} are listed in Table I. The average resistance of the pinholes in 7 skin samples corresponds to 180 μm for d_{hole} (range from 126 to 241 μm). If the hole resistance of 19.76 kΩ (sample 2) is discarded as an outlier, then the average value for R_{hole} is 10.25±2.80 kΩ, which corresponds to 189 μm for d_{hole} (range from 150 μm to 241 μm). Overall, these estimates for d_{hole} are a little smaller than half of the needle diameter (464 μm). This is not surprising since the hole left by pushing a needle through the skin will certainly be smaller than the needle diameter.

Effective Capacitance

Values of the effective capacitance, $C_{s,HM}/A$, calculated using Eqs. (5) and (10) respectively for skin before and after pinhole, are presented in Table III. Before pinhole damage, $C_{s,HM}/A$ was 24.4±2.6 nF/cm^2 (mean ± one standard deviation for 7 samples from two subjects), which was larger than after pinhole damage (16.2±1.6 nF/cm^2) by a statistically significant amount. The magnitude of these results generally agree with other measurements of $C_{s,HM}/A$ reported for human skin; *e.g.*, 18.6 nF/cm^2 for heat separated skin in 50 mM buffered $CaCl_2$ at 32°C (23), 39.8 nF/cm^2 for 145 samples of split-thickness skin in PBS at 32°C (36). Comparable effective capacitance results calculated without an initial evaluation in terms of a CPE are also reported for human as well full-thickness mouse skin; *e.g.*, 8.9 nF/cm^2 for heat separated human skin in 0.0034 M NaCl at 21°C (7), 24 nF/cm^2 for nude mouse in buffered 0.133 M NaCl at 37° (11), and 48, 51, 60 and 67 nF/cm^2 for hairless mouse at 20, 30, 40 and 50°C in 0.1 M NaCl with similar numbers for 0.01 and 1 M NaCl (10).

The effective dielectric constant (ε) for skin can be calculated from the skin capacitance as

$$\varepsilon = \frac{(C_s/A)L}{\varepsilon_0} \tag{18}$$

where L is the stratum corneum thickness (assumed to be 15 μm) and ε_0 is the permittivity of vacuum (8.8542×10^{-5} nF/cm). Significantly, the values of ε calculated using $C_{s,HM}/A$ (listed in Table III as ε_{HM}) are physically unrealistic: 414±44 and 274±28 for skin before and after pinhole damage, respectively. These numbers are one to two orders of magnitude larger than the expected range between 76 for water at 32°C (37) and 2 or 3 for several oils. Presented differently, the capacitance of 15-μm thick films of water and oil are respectively 4.5 and 0.12 nF/cm^2, which is much smaller than the effective skin capacitance estimates. The fact that measurements reported for skin capacitance correspond to physically unrealistic values of ε seems to have gone unnoticed with one exception: DeNuzzio and Berner (7) observed that skin capacitance (calculated by fitting the impedance response to an R-C model circuit) was about 8 nF compared with their theoretical estimate of 0.08 nF (incorrectly listed as 0.8 nF in their Eq. 1).

Recognizing that dielectric constant values estimated from $C_{s,HM}$ are impossibly large, the validity of $C_{s,HM}$ to represent skin capacitance must be questioned. Further evidence that $C_{s,HM}$ is an incorrect measure of skin's dielectric properties is the observation that $C_{s,HM}/A$ consistently changed in all seven skin samples after adding a pinhole, an action that would not have changed the dielectric constant of the skin.

Recently, Hirschorn *et al.* (38) proposed a different approach for estimating the dielectric constant of a material with impedance behavior that is consistent with an R-CPE circuit model. Under the assumption that the dielectric constant is independent of position, they demonstrate that the behavior of an R-CPE circuit is consistent with a power-law decay of skin resistivity through the skin thickness. Based on their power-law model (*cf.* Eqs. 28 and 29 in (38)), an alternative expression for the effective capacitance ($C_{s,PL}$) can be derived (39) as:

$$C_{s,PL}/A = g^{1/\alpha_s}(Q_s/A)^{1/\alpha_s}(\delta\,\rho_\delta)^{(1-\alpha_s)/\alpha_s} \tag{19}$$

where ρ_δ is the resistivity at the position, δ, of the innermost interface of the dominant resistive layer (*i.e.*, the stratum corneum in the case of skin) and the parameter g is obtained from

$$g = 1 + 2.88(1-\alpha_s)^{2.375} \tag{20}$$

For α_s between 0.8 and 0.9, which are typical values for skin, g is between 1.06 and 1.01. Although ρ_δ is unknown, to satisfy the assumption that skin properties do not change after needle puncture, ρ_δ and also $C_{s,PL}$ and L are constants, and therefore, according to Eq. (19), both Q_s and α_s must also

Table III Comparing Capacitance and Dielectric Constant Values Calculated Before and After Damage with One Pinhole Using the Power-Law (PL) and Hsu-Mansfeld (HM) Models

Sample ID	α_s [a]	Q_s/A [a] nF s^{α_s-1}/cm^2	$C_{s,PL}$ [b] nF/cm^2	ε_{PL}	$C_{s,HM}$ [b] nF/cm^2		ε_{HM}	
					Before	After	Before	After
1	0.815	73.8	1.07	18.2	26.2	14.3	444	243
2	0.820	71.0	1.17	19.9	23.6	18.0	400	297
3	0.805	91.4	1.06	17.9	28.8	18.8	488	318
4	0.830	65.1	1.39	23.5	20.6	15.0	348	254
5	0.840	56.6	1.53	25.9	23.6	14.8	399	251
6	0.825	63.9	1.18	20.0	25.1	15.7	426	267
7	0.825	71.9	1.37	23.1	23.3	16.9	395	285
Mean	0.823	70.5	1.25	21.2	24.5	16.2	414	274
Std dev	0.011	10.9	0.18	3.0	2.6	1.6	44	28

[a] Reported values for α_s and Q_s/A are the average of the before and after pinhole values because these were not statistically significantly different

[b] $C_{s,PL}$ and $C_{s,HM}$ were calculated according to Eqs. (19) and (5), respectively using the average of the before and after pinhole values for α_s and Q_s/A; $C_{s,PL}$ was calculated for $\rho_\delta = 55\ \Omega$ cm and $\delta = 15\ \mu$m

remain constant. Notably, this theoretical prediction is consistent with experimental observations that Q_s and α_s before and after pinhole were not statistically significantly different.

A further test of the validity of $C_{s,PL}$ for representing skin capacitance is to compare the predicted and observed changes in the characteristic frequency after adding a pinhole to skin. Since constant ε means that Q_s and α_s do not change, then, according to Eqs. (3) and (8), the ratio of the characteristic frequencies before-to-after pinhole damage is predicted to be related to the before-to-after resistance ratio as:

$$\left(\frac{f_{c,s}}{f_{c,t}}\right)\left(\frac{R_s}{R_t}\right)^{1/\alpha_s} = 1 \tag{21}$$

This differs from what is predicted for the $C_{s,HM}$ approach if ε does not change. If ε does not change, then $C_{s,HM}$ does not change and according to Eqs. (4) and (9), the ratio of the characteristic frequencies and resistances are expressed as:

$$\left(\frac{f_{c,s}}{f_{c,t}}\right)\left(\frac{R_s}{R_t}\right) = 1 \tag{22}$$

As shown in Fig. 5, Eq. (21) is consistent with the experimental observations, while Eq. (22) is not. This result supports the hypothesis that $C_{s,HM}$ does not reflect accurately the effective dielectric constant of the skin.

Estimates of ε from the power-law model are only possible if δ and ρ_δ in Eq. (19) are known. The smallest possible value for ρ_δ may be assumed to be the resistivity of the solution, which was 55 **Ω** cm. Using this, which will give the smallest possible value for $C_{s,PL}$, and an estimate of the thickness of the stratum corneum (15 μm) for δ, $C_{s,PL}$ for the 7 skin samples were calculated along with ε_{PL} (see Table III) for α_s and Q_s/A equal to the average of their before and after pinhole values (which were not statistically significantly different). The result is $C_{s,PL} = 1.2 \pm 0.2$ nF/cm^2, which gives ε_{PL} (21 ± 3) within the expected range of 2 to 76. Because ρ_δ may be larger than the resistivity of the solution, the actual values for ε_{PL} may be larger. Notably, an increase in ρ_δ from the solution resistance of 55 **Ω** cm to as high as 1,000 **Ω** cm produces only a modest increase in ε_{PL} from 21 to 40 at the average values of Q_s/A (70.5 nF s^{α_s-1}/cm^2) and α_s (0.82) for the seven skin samples before pinhole damage. These values of the dielectric constant can be compared to the range of values between 29 and 53 obtained in different studies by a technique which measures absorption and reflection of electromagnetic energy at a radiofrequency of 300 MHz (40, 41).

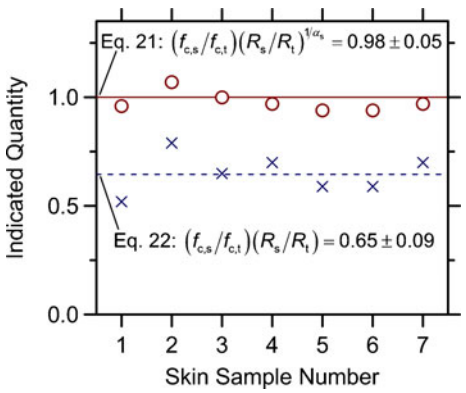

Fig. 5 Experimental values for the ratios of the characteristic frequencies and resistances before and after pinhole damage as predicted by two different approaches for calculating the effective capacitance from the R-CPE parameters: (**a**) the power-law model (Eq. (21)), represented as circles, and (**b**) the Hsu-Mansfeld model (Eq. (22)) represented as X. Because pinhole damage does not change the skin dielectric constant, the expressions should be 1, which is observed for the power-law model but not for the Hsu-Mansfeld model.

Table IV Steady-State Flux of CP ($\mu g/cm^2/h$) Measured Before and After Damage with One Pinhole

	Sample ID[a]								All samples[b]	
	Control	1	2	3	4	5	6	7	Mean	Std dev
Before	0.164	101.8	109.8	134.5	107.6	50.9	58.5	55.4	88.4	33.0
After	0.164	120.0	135.4	149.1	127.2	61.8	62.2	62.0	102.5	38.9
Change[c]	0	18.2	25.6	14.5	19.6	10.9	3.7	6.5	14.1	7.7
% Change[c]	0	17.9	23.3	10.9	18.2	21.4	6.3	11.9	15.7	6.2

[a] Samples 1–4 are from subject Q; samples 5–7 are from subject AS. After pinhole, $R_t A > 20\ k\Omega\ cm^2$ for only samples 2 and 6

[b] Values are the mean ± one standard deviation of the parameter values for all seven skin samples

[c] Change is the flux after treatment minus the flux before treatment; % Change is the change in flux divided by the flux before pinhole

Other methods have been used to extract effective capacitance values directly from skin impedance data without an initial evaluation in terms of a CPE. Generally, the results from these methods have been consistent with each other and with $C_{s,HM}$. In the simplest approach, the effective capacitance was determined by assuming skin impedance was represented by the R-C circuit model; *e.g.*, (7, 19, 42). Capacitance values estimated by fitting the R-C circuit model to skin, which behaves like an R-CPE circuit, will be equal to $C_{s,HM}$ because the regressed R-C model parameters will have the same characteristic frequency as a regression to the R-CPE circuit. Oh and Guy (43, 44) estimated the effective capacitance ($C_{s,OG}$) using the formula

$$C_{s,OG} = \frac{\tan\theta_{c,s}}{2\pi R_s f_{c,s}} \tag{23}$$

where $\theta_{c,s}$ is the phase angle at the characteristic frequency ($f_{c,s}$). Oh and colleagues (9, 10) and also Burnette and Bagniefski (11) determined the effective capacitance ($C_{s,Oh}$) from the slope of the a linear regression of the inverse of the modulus of the impedance squared $|Z|^2$ to the frequency as described by

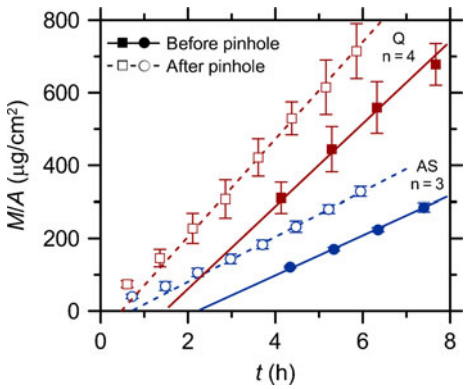

Fig. 6 Cumulative permeation of CP through human skin from subjects Q (*squares*) and AS (*circles*) before (*filled symbols*) and after (*open symbols*) damage with one pinhole; error bars representing plus or minus one standard deviation are not always visible. *Lines* represent the average steady-state permeation for each subject before (*solid*) and after (*dashed*) pinhole damage.

$$\frac{1}{|\tilde{Z}|^2} = \frac{1}{R_s^2} + C_{s,Oh}^2(4\pi^2)f^2 \tag{24}$$

for frequencies close to $f_{c,s}$. The effective capacitance values calculated using these methods are related to $C_{s,HM}$ as (see derivations in the Supplementary Material)

$$C_{s,OG} = C_{s,HM}\tan(\alpha_s\pi/4) \tag{25}$$

$$C_{s,Oh} = C_{s,HM}(f/f_{c,s}) \tag{26}$$

This explains why the values generated from these methods are similar to $C_{s,HM}$ and, like $C_{s,HM}$, give physically unreasonable estimates for the dielectric constant.

Chemical Flux

The steady-state fluxes of CP before and after damage and the change in CP flux after damage are listed in Table IV. Under the assumption that all seven samples belong to the same population, the CP flux after pinhole is not significantly different than before pinhole. However, samples 1–4 (mean flux was $113 \pm 14\ \mu g/cm^2/h$ before the pinhole) were from a different subject than samples 5–7 (mean flux was $55 \pm 4\ \mu g/cm^2/h$ before pinhole). The average cumulative permeation measured before and after pinhole damage for each subject is presented in Fig. 6. Lag times before the pinhole were larger than after the pinhole because the skin in the before pinhole measurement had not been exposed previously to CP. For each subject the mean CP flux after pinhole was larger than the CP flux before pinhole by a small but statistically significant amount (student *t*-test, $p < 0.05$) with a percentage change that was similar for both subjects (16% ± 6% for all samples). As an experimental control, one sample was treated in the same way as the pinhole samples except no pinhole was made. The CP flux for the control sample did not change (Table IV), suggesting that the observed changes in flux were due only to the hole or to changes in the skin incurred while making the hole. Despite this, the change in CP flux was not correlated with either the hole resistance or

diameter, perhaps because the variation in the values of the after pinhole resistances were too small relative to the experimental variability of flux through intact skin.

A minimum resistance of 20 kΩ cm^2 has been recommended as a criterion for skin samples with acceptable skin integrity for meaningful measurement of *in-vitro* chemical permeability without screening undamaged but higher permeability samples from the study; *e.g.*, see discussion in (6). By this criterion five samples damaged with one pinhole exhibited unacceptable integrity (9 to 16 kΩ cm^2), and two samples, one from each subject, were barely acceptable (21 and 24 kΩ cm^2). Consistent with the observations described above, the two acceptable samples exhibited both the highest and lowest percentage changes respectively for subjects Q and AS. The observation that CP flux changed by only a small amount when the resistance of the pinhole damaged skin sample was close to or slightly less than 20 kΩ cm^2 suggests that this criterion is an adequate assessment of skin quality for permeation measurements of non-polar compounds.

Skin damaged intentionally with multiple holes to increase chemical permeation (as in treatments with microneedles, electroporation, or thermal, radiofrequency or laser ablation (45, 46)) often will exhibit resistances that are less than 1 kΩ cm^2; *e.g.*, (47). The amount of skin damage after such treatments probably is large enough to cause an observable increase in the flux of non-polar compounds like CP that are not too lipophilic. However, permeation enhancement for highly soluble polar and ionized species or for larger molecules that have extremely limited permeability through undamaged SC should be more significant and correlated with the skin resistance measured after treatment (48).

CONCLUSIONS

Skin impedance measurements are sensitive to irreversible damage caused by puncture with a needle, which reduced the average resistance almost 10 fold. Skin impedance before and after pinhole damage is represented well by an R-CPE circuit model that is characterized by a single characteristic frequency. Pinhole damage adds a low frequency shunt resistance through the hole that acts in parallel with the skin resistance, but does not change the CPE parameters. The characteristic frequency of the impedance scans determined after needle puncture increased by more than the decrease in the total resistance. This is inconsistent with approaches that have been used previously to estimate an effective skin capacitance from the R-C equivalent circuit model. The measured increases in the characteristic frequency were consistent with the theory from Hirschorn *et al.* (23), which predicts that the CPE parameters of the skin (α_s and Q_s) should not change if the dielectric constant and resistivity are constant. After pinhole damage, the flux of CP did increase by a small but significant amount. However, this increase was not correlated with the hole resistance or diameter estimated by assuming that the skin resistance was unchanged after the pinhole. The detailed analysis in the present work was made possible by the measurement of impedance over a broad range of frequency that encompassed both the high frequencies where capacitive effects dominated to low frequencies that allowed estimation of steady-state resistances.

ACKNOWLEDGMENTS AND DISCLOSURES

The authors acknowledge support from the National Institute of Occupational Safety and Health (application number 1-R01-OH007493).

REFERENCES

1. Barry BW, Bennett SL. Effect of penetration enhancers on the permeation of mannitol, hydrocortisone and progesterone through human-skin. J Pharm Pharmacol. 1987;39(7):535–46.
2. Kasting GB, Bowman LA. Dc electrical properties of frozen, excised human skin. Pharm Res. 1990;7(2):134–43.
3. Peck KD, Ghanem AH, Higuchi WI. Hindered diffusion of polar molecules through and effective pore radii estimates of intact and ethanol treated human epidermal membrane. Pharm Res. 1994; 11(9):1306–14.
4. Peck KD, Ghanem AH, Higuchi WI. The effect of temperature upon the permeation of polar and ionic solutes through human epidermal membrane. J Pharm Sci. 1995;84(8):975–82.
5. Tang H, Mitragotri S, Blankschtein D, Langer R. Theoretical description of transdermal transport of hydrophilic permeants: application to low-frequency sonophoresis. J Pharm Sci. 2001;90(5):545–68.
6. White EA, Horne A, Runciman J, Orazem ME, Navidi WC, Roper CS, *et al.* On the correlation between single-frequency impedance measurements and human skin permeability to water. Toxicol *In Vitro*. 2011;25(8):2095–104.
7. DeNuzzio JD, Berner B. Electrochemical and iontophoretic studies of human skin. J Control Release. 1990;11(1–3):105–12.
8. Curdy C, Kalia YN, Guy RH. Non-invasive assessment of the effects of iontophoresis on human skin *in-vivo*. J Pharm Pharmacol. 2001;53(6):769–77.
9. Kim HS, Oh SY. Effect of polyoxyethylene alkyl esters on permeation enhancement and impedance of skin. Biomol Ther. 2011;19(1):109–17.
10. Oh SY, Leung L, Bommannan D, Guy RH, Potts RO. Effect of current, ionic strength and temperature on the electrical properties of skin. J Control Release. 1993;27(2):115–25.
11. Burnette RR, Bagniefski TM. Influence of constant current iontophoresis on the impedance and passive Na+permeability of excised nude mouse skin. J Pharm Sci. 1988;77(6):492–7.
12. Heylings JR, Esdaile DJ. Percutaneous absorption of pesticides. In: Roberts MS, Walters KA, editors. Dermal absorption and toxicity assessment. 2nd ed. New York: Informa Healthcare; 2007. p. 575–91.
13. International Programme on Chemical Safety (IPCS). Dermal absorption, environmental health criteria 235. Geneva: World Health Organization; 2006.
14. OECD. OECD guideline for testing of chemicals. Guideline 428: Skin absorption: *In vitro* method (original guideline, adopted 13th April 2004); 2004.

15. White EA, Orazem ME, Bunge AL. Characterization of damaged skin by impedance spectroscopy: Chemical damage by dimethyl sulfoxide. Pharm Res. 2013. In Press.
16. Yamamoto T, Yamamoto Y. Non-linear electrical-properties of skin in the low-frequency range. Med Biol Eng Comput. 1981; 19:302–10.
17. Salter DC. Examination of stratum corneum hydration state by electrical methods. In: Elsner P, Barel AO, Berardesca E, Gabard B, Serup J, editors. Skin bioengineering: Techniques and applications in dermatology and cosmetology. Basel: Karger Publishers; 1998. p. 38–47.
18. Jorcin J-B, Orazem ME, Pébère N, Tribollet B. CPE analysis by local electrochemical impedance spectroscopy. Electrochim Acta. 2006;51:1473–9.
19. Yamamoto T, Yamamoto Y. Electrical properties of the epidermal stratum corneum. Med Biol Eng. 1976;14(2):151–8.
20. Yamamoto T, Yamamoto Y. Dielectric constant and resistivity of epidermal stratum corneum. Med Biol Eng Comput. 1976;14: 494–500.
21. Hsu CH, Mansfeld F. Technical note: concerning the conversion of the constant phase element parameter Y_0 into a capacitance. Corrosion. 2001;57(9):747–8.
22. Orazem ME, Pébère N, Tribollet B. Enhanced graphical representation of electrochemical impedance data. J Electrochem Soc. 2006;153(4):B129–36.
23. Hirschorn B, Orazem ME, Tribollet B, Vivier V, Frateur I, Musiani M. Determination of effective capacitance and film thickness from constant-phase-element parameters. Electrochim Acta. 2010;55(21):6218–27.
24. Bunge AL, Cleek RL, Vecchia BE. A new method for estimating dermal absorption from chemical exposure. 3. Compared with steady-state methods for prediction and data analysis. Pharm Res. 1995;12(7):972–82.
25. Pratt KW, Koch WF, Wu YC, Berezansky PA. Molality-based primary standards of electrolytic conductivity - (IUPAC technical report). Pure Appl Chem. 2001;73(11):1783–93.
26. Gavin H. The Levenberg-Marquardt method for nonlinear least squares curve-fitting problems: Department of Civil and Environmental Engineering, Duke University, p. 15; 2011.
27. Orazem ME, Tribollet B. Electrochemical impedance spectroscopy. Hoboken: Wiley-Interscience; 2008.
28. Agarwal P, Orazem ME, Garcia-Rubio LH. Measurement models for electrochemical impedance spectroscopy 1. Demonstration of applicability. J Electrochem Soc. 1992;139(7):1917–26.
29. Agarwal P, Crisalle O, Orazem ME, Garcia-Rubio L. Application of measurement models to impedance spectroscopy, II. Determination of the stochastic contribution to the error structure. J Electrochem Soc. 1995;142(12):4149–58.
30. Agarwal P, Orazem ME, Garcia-Rubio L. Application of measurement models to impedance spectroscopy, III. Evaluation of consistency with Kramers-Kronig relations. J Electrochem Soc. 1995;142(12):4159–68.
31. Agarwal P, Orazem ME, Garcia-Rubio LH. The influence of error structure on interpretation of impedance spectra. Electrochim Acta. 1996;41(7/8):1017–22.
32. Orazem ME, Moustafid TE, Deslouis C, Tribollet B. The error structure of impedance spectra for systems with a large ohmic resistance with respect to the polarization impedance. J Electrochem Soc. 1996;143(12):3880–90.
33. Orazem ME. User manual for the measurement model toolbox for impedance spectroscopy. Gainesville: University of Florida; 2001.
34. Carslaw HS, Jaeger JC. Conduction of heat in solids. Oxford: Oxford University Press; 1959.
35. Newman JS. Resistance for flow of current to a disk. J Electrochem Soc. 1966;113:501–2.
36. White EA, Orazem ME, Bunge AL. A critical analysis of single-frequency LCR databridge impedance measurements of human skin. Toxicol *In Vitro*. 2011;25(4):774–84.
37. Groen D, Gooris GS, Bouwstra JA. Model membranes prepared with ceramide EOS, cholesterol and free fatty acids form a unique lamellar phase. Langmuir. 2010;26(6):4168–75.
38. Hirschorn B, Orazem ME, Tribollet B, Vivier V, Frateur I, Musiani M. Constant-phase-element behavior caused by resistivity distributions in films I. Theory. J Electrochem Soc. 2010;157(12):C452–7.
39. Orazem ME, Frateur I, Tribollet B, Vivier V, Marcelin S, Pébère N, *et al.* Dielectric properties of materials showing constant-phase-element (CPE) impedance response. J Electrochem Soc. 2013.
40. Petäjä L, Nuutinen J, Uusaro A, Lahtinen T, Ruokonen E. Dielectric constant of skin and subcutaneous fat to assess fluid changes after cardiac surgery. Physiol Meas. 2003;24(2):383–90.
41. Jensen MR, Birkballe S, Norregaard S, Karlsmark T. Validity and interobserver agreement of lower extremity local tissue water measurements in healthy women using tissue dielectric constant. Clin Physiol Funct Imaging. 2012;32(4):317–22.
42. Allenby AC, Fletcher J, Schock C, Tees TFS. The effect of heat, pH and organic solvents on the electrical impedance and permeability of excised human skin. Br J Dermatol. 1969;81(4):31–9.
43. Oh SY, Guy RH. The effect of oleic acid and propylene glycol on the electrical properties of skin. J Korean Pharm Sci. 1994;24(4):281–7.
44. Oh SY, Guy RH. Effect of enhancers on the electrical properties of skin: the effect of azone and ethanol. J Korean Pharm Sci. 1994;24(3):S41–7.
45. Prausnitz MR, Langer R. Transdermal drug delivery. Nat Biotechnol. 2008;26(11):1261–8.
46. Banga AK. Microporation applications for enhancing drug delivery. Expert Opin Drug Deliv. 2009;6:343–54.
47. Brogden NK, Milewski M, Ghosh P, Hardi L, Crofford LJ, Stinchcomb AL. Diclofenac delays micropore closure following microneedle treatment in human subjects. J Control Release. 2012;163(2):220–9.
48. Milewski M, Brogden NK, Stinchcomb AL. Current aspects of formulation efforts and pore lifetime related to microneedle treatment of skin. Expert Opin Drug Deliv. 2010;7(5):617–29.